Effects of electrostatic fields and charge doping on the linear bands in twisted graphene bilayers

Lede Xian, Salvador Barraza-Lopez, and M. Y. Chou

Phys. Rev. B **84**, 075425 — Published 5 August 2011

DOI: 10.1103/PhysRevB.84.075425

Effect of electrostatic fields and charge doping on the linear bands in twisted graphene bilayers

Lede Xian,[1] Salvador Barraza-Lopez,[1] and M. Y. Chou[1,2]

[1]*School of Physics, Georgia Institute of Technology, Atlanta, Georgia 30332, USA*
[2]*Institute of Atomic and Molecular Sciences, Academia Sinica, Taipei 10617, Taiwan*

A twisted graphene bilayer consists of two graphene monolayers rotated by an angle θ with respect to each other. Theory predicts that charge-neutral twisted graphene bilayers display a drastic reduction of their Fermi velocity v_F for $0 \lesssim \theta \lesssim 20^\circ$ and $40 \lesssim \theta \lesssim 60^\circ$. In this paper we present evidence for an additional anisotropic reduction of v_F in the presence of external electrostatic fields. We also discuss in quantitative detail velocity renormalization for other relevant bands in the vicinity of the K point. Except for a rigid energy shift, electrostatic fields and doping by metal atoms give rise to similar renormalization of the band structure of twisted graphene bilayers.

PACS numbers: 73.22.Pr, 73.21.Ac

I. INTRODUCTION

Graphene is a two-dimensional zero-gap material with carbon atoms arranged in a honeycomb lattice. It has outstanding electronic, optical and mechanical properties[1,2] with charge carriers exhibiting a linear dispersion that can be described by a relativistic Dirac-Weil equation. Bulk graphite is formed when graphene layers are stacked following a well-defined (Bernal) pattern. In contrast, graphene layers grown by silicon sublimation on SiC$(000\bar{1})$[3,4] or by chemical vapor deposition (CVD) on metal substrates[5,6] contain rotational faults or "twists"[7] between successive layers. The electronic structure of these twisted graphene multilayers differs from that of graphite and displays linear bands close to the charge neutrality level.[4,8,9] Few-layer graphene with rotational faults is arguably a promising material for a number of device applications, including field-effect transistors,[10–12] resistance standards,[13] and transparent electrodes.[14,15]

Band structure calculations on bilayer graphene with rotational faults, the so-called "twisted graphene bilayer" (TGB), confirm the persistence of the linear dispersion[7,16–19] down to tens of meVs away from the charge neutrality point,[20] with no gap opening under transverse electric fields.[7,21] This is markedly different from the Bernal-stacked bilayer, where a tunable electronic gap is created by transverse electrostatic fields.[22,23] Starting from a Bernal-stacked graphene bilayer, a TGB is formed by rotating the upper layer about the overlapping A-sublattice by an angle θ with respect to the lower layer. Commensurate structures labeled by (m,n) correspond to a rotational angle of θ satisfying the condition:[7,17,18,20]

$$\cos(\theta) = \frac{n^2 + 4nm + m^2}{2(n^2 + nm + m^2)}. \tag{1}$$

The lattice vectors of the TGB supercell are $\mathbf{t}_1 = n\mathbf{a}_1 + m\mathbf{a}_2$, and $\mathbf{t}_2 = -m\mathbf{a}_1 + (n+m)\mathbf{a}_2$, where $\mathbf{a}_1$ and $\mathbf{a}_2$ are the lattice vectors of the primitive unit cell in monolayer graphene ($|\mathbf{a}_1| = a_0$).

A drastic reduction of the Fermi velocity v_F in TGBs with respect to that of monolayer graphene v_{F0} has been predicted for small θ.[7,18,19,24] A transition from a parabolic (Bernal) to a linear dispersion[24] sets in at θ values somewhere between 0° and 2° (or 58° and 60°). For extremely small values of θ, complex behavior is expected.[19,25,26] The electronic coupling for low energy bands between layers in a TGB differs from that in a Bernal bilayer, since the coupling takes place, to the first order, between states near the Dirac point in one layer and those in the other layer at energies $\pm E_c$,[7] with:

$$E_c(\theta) = \hbar v_{F0} \Delta K = 2\hbar v_{F0} |K| \sin(\theta/2), \tag{2}$$

where $|K| = 4\pi/3a_0$. In Bernal bilayer the coupling occurs for states at the *same* energy. Besides the velocity renormalization for small values of θ and the lack of gap opening in transverse electrostatic fields, little has been reported for TGBs under electrostatic fields or charge doping.

On the experimental side, values for v_F obtained by a host of techniques on various types of samples are scattered. Raman spectroscopy seemed to indicate[27–29] a 5% reduction of the Fermi velocity in folded graphene. Early transport experiments[3] gave $v_F/v_{F0} = 0.66$ in folded graphene and $v_F/v_{F0} = 0.7$ in epitaxial graphene (EPG) grown on SiC$(000\bar{1})$. ARPES[9] and STM[30] measurements on other EPG samples yielded $v_F/v_{F0} = 1.0$. High magnetic field STM topography and Landau level spectroscopy had been combined to study graphene twisted layers grown by CVD showing a strong angle-dependent Fermi velocity renormalization,[31] in quantitative agreement with theoretical

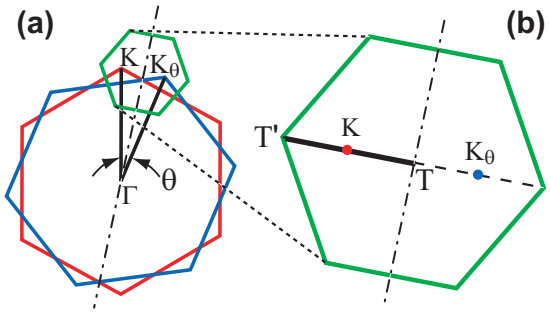

FIG. 1: (Color online) (a) The large hexagons indicate the Brillouin zone of each of the two rotated layers, while the small hexagon illustrates the size of the Brillouin zone for the twisted graphene bilayer. (b) The small hexagon in (a) is magnified to indicate the $T - T'$ segment over which the band structures are discussed in this work. The band structure is symmetric with respect to the dash-dot line, so that energy bands at the K_θ and K points are the same.

predictions. Recent ARPES investigations on graphene layers grown on SiC(000$\bar{1}$) yielded $v_F/v_{F0} \cong 1.0$ for all the samples studied.[32]

While theoretical studies have assumed charge neutral TGB, many experimental graphene multilayer systems have certain degree of doping[9,30,32] by the substrate,[33] by extraneous contamination, or intentionally produced.[34–40] This shifts the location of the Fermi level and induces a potential difference across layers. In this work, we study in detail the effect of electrostatic potential or doping on the electronic energy bands in TGBs using density functional theory (DFT) and tight-binding calculations beyond the first-order analytical results in Ref. 7. We have identified an enhanced, anisotropic reduction of v_F with an on-site perturbation $\Delta E/2$ ($-\Delta E/2$) applied to the upper (lower) layer. Additionally, when $\Delta E \geq E_c$ we find that linear bands with velocities close to v_{F0} reappear away from the Fermi level. This is corroborated by k-point resolved charge population analysis in each layer indicating almost single layer occupation. Calculations with charge doping are shown to reproduce this behavior on TGBs induced by the relative on-site energy shifts between layers, with the additional advantage of resetting the location of the Fermi level.

The paper is organized as follows: In Sec. II we summarize the calculational details. In Section III A we discuss the band structure for an (8,9) TGB ($\theta = 3.89°$) and a (14,15) TGB ($\theta = 2.28°$) as ΔE varies. We then present the velocities of linear bands in TGBs as a function of ΔE and θ and discuss the identified trends. In Section III B we investigate an (8,9) TGB under charge doping. We offer conclusions in Sec. IV.

II. CALCULATIONAL DETAILS

We perform DFT calculations on TGBs under transverse electrostatic fields or charge doping. Our calculations are carried out within the local-density approximation (LDA)[41,42] with the SIESTA package,[43,44] in which the valence electrons are described with Troullier-Martins pseudopotentials[45] and a set of localized numerical atomic orbitals.[46] In addition, tight-binding calculations are performed for π electrons with up to third nearest-neighbors in-plane hopping (with $\gamma_0 = 2.80$ eV) and a separate, exponentially decaying inter-plane hopping term with $\gamma_1 = 0.42$ eV ($q_\pi = 3.15$ and $q_\sigma = 7.48$; see Ref. 19 for more details). We use the wave functions from the tight-binding calculations to compute the layer population $\sigma_j(\mathbf{k})$ for a given eigenstate j at a specific $\mathbf{k}$-point, defined as:

$$\sigma_j(\mathbf{k}) = \frac{\sum_{i \in LM} |\Psi_j(i,\mathbf{k})|^2}{\sum_l |\Psi_j(l,\mathbf{k})|^2}, \tag{3}$$

where i and l denote atomic sites and Ψ is the tight-binding expansion coefficient. The sum in the numerator runs over only the lower monolayer (LM), while the sum in the denominator runs unrestrictedly over all atoms in the supercell. $\sigma_j(\mathbf{k})$ is zero (one) if only the orbitals in the the upper (lower) layer are populated. In general, $0 \leq \sigma_j(\mathbf{k}) \leq 1$.

In this paper we focus on (m,n) TGBs satisfying $m = n + 1$ ($n > 0$). This is one of the two families of TGBs as described by Mele[20] with a one-to-one correspondence between n and θ. The DFT calculations are carried out in the presence of charge dopants or electrostatic fields. We focus on systems for which the Fermi velocity v_F is renormalized by at least 20% with respect to v_{F0}, namely, $\theta < 10°$ according to Refs. 7 and 19 in order to investigate any additional renormalization induced by the electrostatic field or doping. The structural parameters used are $a_0 = 2.42$ Å and $d = 3.35$ Å.

The first Brillouin zones of the top and rotated bottom layers are shown in Fig. 1(a). The small hexagon illustrates the size of the Brillouin zone for the TGB supercell. It is amplified in Fig. 1(b) in order to indicate the line T-T' in

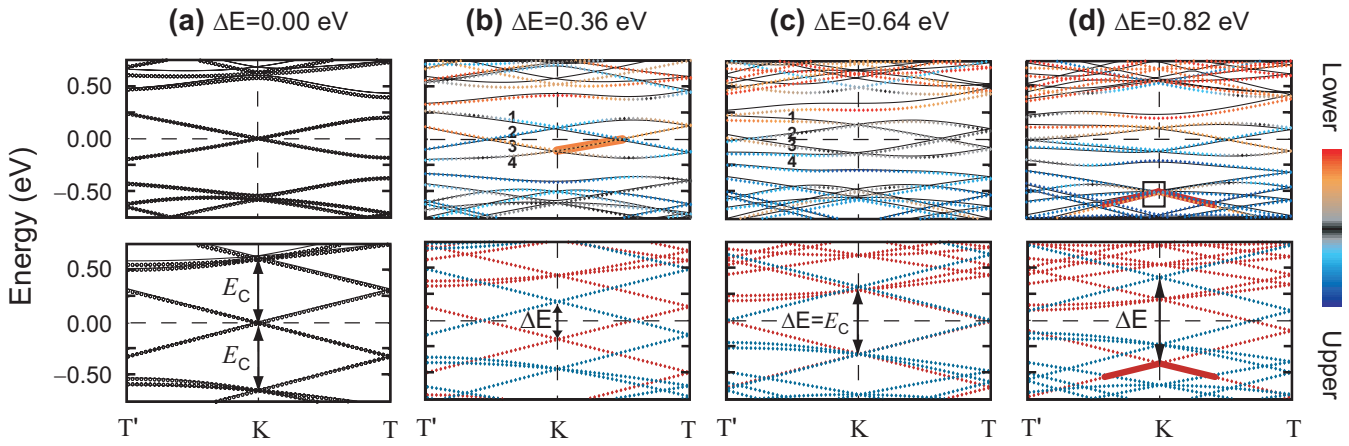

FIG. 2: (Color online). Changes of band dispersions for the (8,9) twisted graphene bilayer ($\theta = 3.89°$, $E_c = 0.64$ eV) as the electrostatic field increases. Energies calculated using density functional theory (DFT) are shown by solid lines in the upper row for the following electric fields: (a) 0.0, (b) 0.4, (c) 0.7, and (d) 1.0 eV/Å. For comparison, the dispersions of a single-layer graphene with an (8,9) supercell in zero field are plotted in the lower part of (a). Tight-binding results are shown by symbols; results with (without) the interlayer interaction included are shown in the upper (lower) row; and the on-site energy differences ΔE between the two layers that best describe the results of DFT calculations are indicated. The color coding of the data indicates layer population as defined in Eq. (3), with single-layer population at the extremes of the color bar and equal population in the middle of the color scale. Bands of interest are highlighted with numbers and bold lines. The small rectangle in (d) will be discussed in Fig. 3. The horizontal axis spans the range of $(-0.058, 0.058)$ Å^{-1} in all subplots.

reciprocal space for which the band structure is plotted throughout this paper. The band structure is symmetric with respect to the dash-dot line in Figs. 1(a) and 1(b), and K'_θ (K') is folded back to K (K_θ).

We will discuss two particular groups of bands: The first one corresponds to those studied in Refs. 7 and 19, while the second group lies lower in energy around the K point. In order to provide a measure of the linearity (or lack thereof) of these bands at the vicinity of the K point, we carry out power-law fits on band segments starting at K and ending half-way towards T (or T').

III. RESULTS

A. Band Renormalization by Electrostatic Field

We first consider an (8,9) TGB ($\theta = 3.89°$, $E_c = 0.64$ eV, and $v_F/v_{F0} \simeq 0.8$). In the upper row of Fig. 2, we show the band structures obtained from DFT calculations (solid lines) for the transverse electric fields of 0.0, 0.4, 0.7, and 1.0 eV/Å, respectively. Also shown are the band structures from tight-binding calculations with corresponding on-site energy differences between the two layers: $\Delta E = 0.00$ (open circles), 0.36, 0.64, and 0.82 eV (diamonds), respectively, which are chosen to best fit the DFT results. The on-site entries in the tight-binding Hamiltonian for a given layer are shifted by either $+\Delta E/2$ or $-\Delta E/2$ in order to keep the energy zero at the Fermi level. For comparison, we show in the lower row of Fig. 2 the corresponding tight-binding band structures with the interlayer interaction turned off, resulting in two sets of monolayer bands displaced by $\pm\Delta E/2$. Our calculated band structure with $\Delta E = 0$ in Fig. 2(a) is consistent with those discussed in previous studies:[7,18,19,24] the low-energy isotropic linear dispersion around the K point is preserved in the TGB; and the magnitude of the Fermi velocity v_F is reduced when compared to v_{F0} ($v_{F0} = 0.83 \times 10^6$ m/s in our LDA calculations), a signature of coupling in TGBs with small θ's.[7,19,24] The reduction of v_F is due to the coupling between states in the Dirac cone of one layer and three pairs of states in the Dirac cone of the other layer separated by a finite energy $E_c(\theta)$ as defined in Eq. (2). As will be discussed below, E_c defines a critical energy scale for the evolution of the band structures as ΔE increases.

The band structures for finite ΔE are shown in Fig. 2(b)-(d). The layer population as defined in Eq. (3) is presented by the color scale of the symbols. When $\Delta E < E_c(\theta)$ the on-site energy difference between the layers results in a small perturbation to the band structure. The originally degenerate Dirac cones around the Fermi level in Fig. 2(a) split into two sets of cones, as labeled by 1-4 in Fig. 2(b). Analysis of layer population in Fig. 2(b) confirms that for $\Delta E = 0.36$ eV charge carriers of bands 1 and 2 are mainly localized in the upper layer while carriers of bands 3 and 4

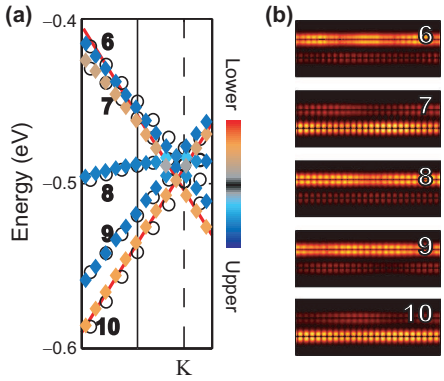

FIG. 3: (Color online). (a) Band structure within the rectangle in Fig. 2(d). The colored diamonds correspond to tight-binding results, and the open circles are from DFT calculations. The (red) lines help stress the linearity of the Dirac cones. The actual data in the upper portion of the plot (above the crossing point) deviates from the linear trend slightly due to hybridization. (b) Charge densities obtained from density-functional-theory calculations for states at the particular k-point indicated by the solid vertical line in (a). These density distributions validate the layer population analysis based on tight-binding results.

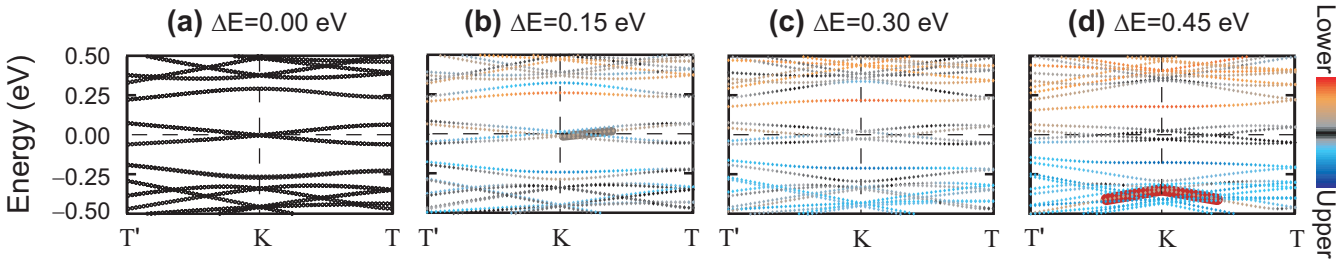

FIG. 4: (Color online). Band structures for the (14,15) TGB ($\theta = 2.28^\circ$, $E_c = 0.38$ eV) calculated by the tight-binding method with various on-site energy differences ΔE between the two layers. The color scheme and highlighted bands are consistent with those presented in the upper row of Fig. 2. The value of ΔE needed to observe the monolayer-like bands on (d) is smaller than the one needed for the (8,9) system. The anisotropic flattening of the bands close to zero energy as ΔE increases is also corroborated. The horizontal axis spans the range of $(-0.035, 0.035)$ Å^{-1} in all subplots.

are mainly localized in the lower layer. The conical structures are quite linear and isotropic. A comparison between the upper and lower plots in Fig. 2(b) elucidates the effect of interlayer interaction. This regime was also discussed in Ref. 21. When $\Delta E \simeq E_c$ bands 1-4 start to become nonlinear and anisotropic, as evidenced by the different slopes to the left and right of the K point in the upper panel of Fig. 2(c). These bands can no longer be described by a Dirac equation with a renormalized velocity. From the layer population analysis one concludes that these bands carry almost equal weight from both layers. The lower panel in Fig. 2(c), in which the interlayer interaction is turned off, indicates that the bands of both layers overlap substantially near K. Therefore, turning on the interlayer interaction leads to strong band hybridization and the resulting departure from linearity and isotropy. Additionally, these bands are significantly *flatter* than those for $\Delta E = 0$ shown in the upper panel of Fig. 2(a). A quantitative analysis will be provided later.

For $\Delta E > E_c(\theta)$ the isotropic cone-like structures near the Fermi level are no longer present, as shown in the upper panel of Fig. 2(d). The original Dirac cone of the lower (upper) layer is shifted down (up) in energy without much distortion in the presence of an external field. The linear dispersion of the Dirac cone associated with the lower layer at about -0.4 eV is highlighted by an inverted "v" in Fig. 2(d), and the region indicated by a rectangle is amplified in Fig. 3(a). The linear and isotropic features are recovered, with the group velocity v_L close to v_{F0}, showing a weak coupling. Layer population analysis in Fig. 3(a) shows that bands become more localized in one layer. This is further verified by the charge density distributions obtained from DFT calculations, shown in Fig. 3(b).

The role of E_c in the response to the electrostatic field can be understood as follows: A strong hybridization among bands persists for $\Delta E \leq E_c$, and this coupling is responsible for the renormalization of the Fermi velocity v_{F0}. For $\Delta E > E_c$ bands away from the energy zero are localized toward individual layers. Monolayer-like behavior is predicted at energy regions $|E| > \Delta E$ where bands from opposite layers do not overlap. Strong coupling persists for energies $|E| \leq \Delta E$.

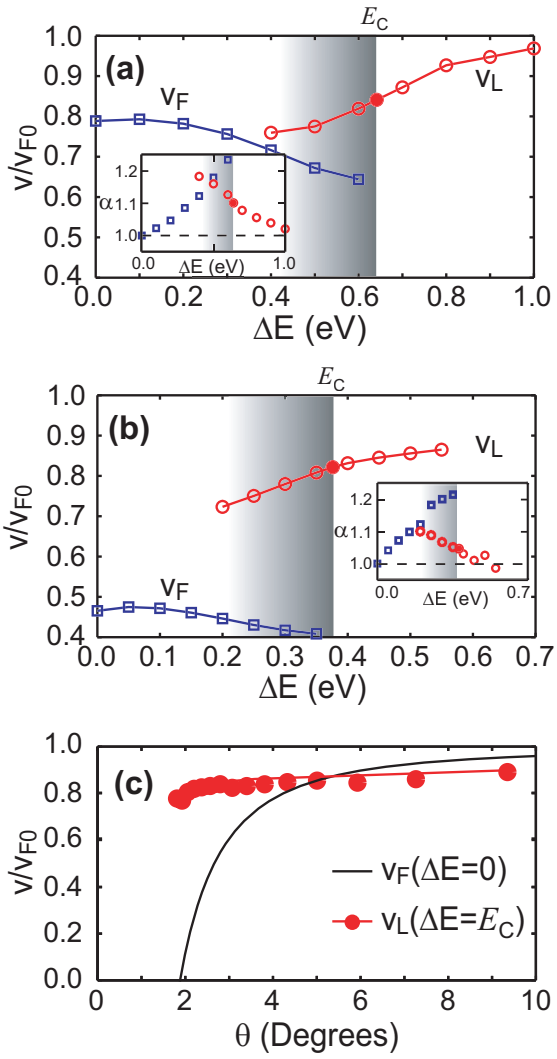

FIG. 5: (Color online). (a) and (b): Amount of band renormalization versus ΔE for the bands highlighted in Fig. 2 and Fig. 4, respectively. The insets show α, the exponent of the power-law fit of the bands of interest. (c) Comparison of the band velocity at the Fermi level v_F for bilayer graphene with $\Delta E = 0$ eV (black line: Ref. 7), and the renormalized velocity of the lower band v_L at $\Delta E = E_c$ (red filled dots; the trend line is only a guide to the eye). Notice that $v_L(E_c) > v_F$ for $\theta \lesssim 5°$.

The results discussed above for the (8,9) TGB ($\theta = 3.89°$) are quite general for other similar or larger θ values. We show in Fig. 4 the tight-binding band structures for the (14,15) TGB ($\theta = 2.28°$, E_c=0.38 eV). Similar results are found: At $\Delta E = 0$, the bands around the Fermi energy are renormalized with $v_F/v_{F0} = 0.45$. As the bias increases the bands crossing the Fermi level gradually become flatter, non-linear, and anisotropic. When ΔE is larger than E_c [Fig. 4(d)] the layer population analysis indicates the presence of predominantly one-layer bands starting from -0.3 eV. We have highlighted the inverted "v" feature, similar to the one displayed in Fig. 2(d), but noticed that a "v" feature in blue (light gray) is also seen at energies $E > 0.30$ eV, also corresponding to weakly coupled Dirac bands. The color scheme and highlighted bands are consistent with those in Fig. 2. The interesting observation is that as θ decreases, the value of ΔE needed for these linear features to reappear *also* becomes smaller, as expected from Eq. (2).

Having established the good agreement between DFT and tight-binding results, in the following we will continue our analysis based on tight-binding calculations. The focus will be on the band segments highlighted with solid thick lines in Figs. 2(b) and 2(d), and in Figs. 4(b) and 4(d). Average band velocities from linear fit as a function of ΔE for these segments are plotted in Fig. 5(a) for the (8,9) TGB and in Fig. 5(b) for the (14,15) TGB, respectively. Power-law fits are performed on data points from K to the midpoint between K and T, which contains a significant and representative number of data points. The insets in Figs. 5(a) and 5(b) show the plot of α, the exponent of the power-law fits. As ΔE increases and approaches E_c, v_F (open blue squares) further *decreases* due to enhanced

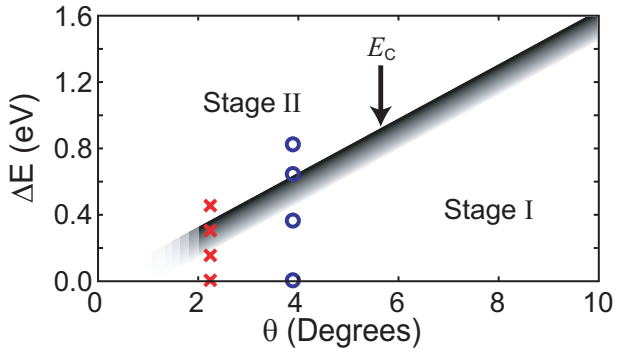

FIG. 6: (Color online) Different stages for evolution of Dirac cones under bias. The open circles and crosses indicate values of θ and ΔE for which band structures were plotted in Figs. 2 and 4. See text for more details.

coupling between states of the two layers. Departure from the linear behavior is noticed as α becomes larger than one as ΔE increases [see the open squares in the insets of Figs. 5(a)-(b)]. In the shaded regions of Figs. 5(a) and 5(b) the coupling is particularly significant that quasiparticle states of those bands near energy zero can no longer be well described as isotropic massless Dirac fermions (see also Fig. 2(c), upper panel and Fig. 4(c)). For $\Delta E > E_c$, the Dirac bands for the lower layer are recovered at an energy location below the Fermi level. The velocity v_L of the charge carriers for this band (open red circles) *increases* with ΔE, approaching v_{F0}. α also approaches one at the same time [see insets in Figs. 5(a)-(b)]. This is a result of weak hybridization with the bands from the upper layer.

We now perform a quantitative investigation of the band dispersion versus the twist angle θ and focus on the same velocity terms discussed above. The results are obtained using the tight-binding method. In Fig. 5(c) we provide a comparative analysis of the renormalization of this lower band at the critical bias value $E_c(\theta)$ [filled red dots in Figs. 5(a) and 5(b)]. We have considered angles corresponding to n = 3, 4, ..., 18 in Eq. (1) in order to examine a large range of twist angles for the general trend to be visible. [Figure 5(c) includes the data points from Figs. 5(a) and 5(b) that are marked with solid circles.] The continuous line $v_F(\Delta E = 0)/v_{F0}$ is from Ref. 7. The velocity for the lower band v_L varies slightly as a function of the twist angle and becomes larger than $v_F(\Delta E = 0)$ for $\theta \lesssim 5°$. We did not extend the calculation down to angles smaller than 2° because a transition between linear bands and parabolic (Bernal) bands is expected for such small rotations.[24] Additional theoretical work on TGBs[7,17–19,24–26,47], outside of the scope of this paper, points to extremely rich behavior for $0° \lesssim \theta \lesssim 2°$ ($58° \lesssim \theta \lesssim 60°$).

We summarize our findings in Fig. 6. The evolution of the band structure versus θ and ΔE can be divided into two broad stages, corresponding to the lower and upper regions separated by the solid line $\Delta E = E_c(\theta)$. In stage I low energy bands resemble Dirac cones with a reduced Fermi velocity v_F. ΔE amounts to an additional relative shift due to the broken symmetry between layers. In stage II, Dirac cones appear in bands sufficiently away from the Fermi level, with their group velocities approaching v_{F0}. There is a intermediate region between stages I and II (shaded region in Fig. 6) where a large overlap between bands of both layers exists, with a resulting strong coupling and subsequent absence of monolayer-like dispersion features.

B. Band Renormalization by Charge Doping

We have also investigated the charge doping effect by metal adatoms on the TGB. Eighteen Al atoms are uniformly distributed over the unit cell area (188 Å^2) of the (8,9) TGB ($\theta = 3.89°$) at a fixed distance $d = 3.3$ Å away from one of the graphene layers. We use this system to create a doping condition in order to assess its impact on the band structure. Therefore, the optimization of adatom positions is not a major concern. We show in Fig. 7 the band structure as the result of this artificial charge doping. The main features include a shift of the Fermi level due to a charge transfer from the Al adatoms to the graphene layers and a splitting of the originally degenerate linear bands associated with the two layers near -0.5 and -0.7 eV. The effect can be reproduced with a tight-binding calculation using $\Delta E = 0.30$ eV and a rigid shift of energies by $\Delta_2 = 0.58$ eV in order to align the bands with the new Fermi level. The tight-binding results (open dots) compare well with the DFT values (solid lines) in Fig. 7. Except for the additional shift of the Fermi level Δ_2, charge doping and electrostatic gating could be considered equivalent methods to induce renormalization of the band velocities in TGBs.

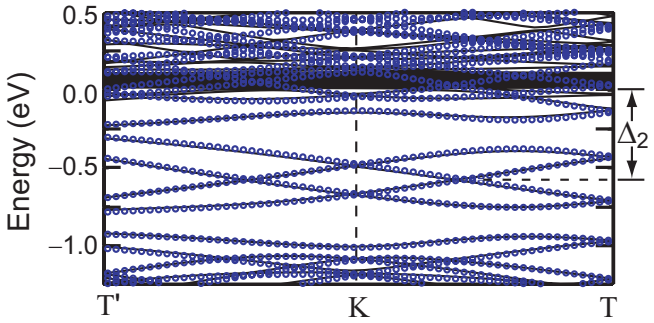

FIG. 7: (Color online). Band structure for the (8,9) twisted graphene bilayer doped with Al atoms: Solid line indicate DFT results and open dots are results of a π-electron tight-binding calculation. The splitting of bands is clearly visible. Besides, the Fermi level is now shifted up by $\Delta_2 = 0.58$ eV with respect to its value on a charge neutral TGB. The horizontal axis spans the range of $(-0.058, 0.058)$ Å^{-1}.

IV. CONCLUSIONS

The epitaxial growth of graphene by silicon sublimation on SiC$(000\bar{1})$ or by chemical vapor deposition on metal surfaces create graphene layers with rotational faults. In the present work, we have studied effects of applied transverse electrostatic fields and charge doping on the energy dispersions of twisted graphene bilayers for angles between 2° and 10° using density functional theory and tight-binding calculations. We have identified: (i) an anisotropic evolution of the Dirac cones near the charge neutrality level; (ii) an additional flattening of these bands; and (iii) the existence of a critical on-site energy difference E_c above which linear and isotropic bands reappear away from the Fermi level, with band velocities approaching that of monolayer graphene. By examining the layer-resolved charge distribution at relevant k points, we confirm a predominant single layer population for these bands. Since E_c decreases with the twist angle θ, the value of ΔE required for these features to appear also decreases with θ. We close our discussion by (iv) providing a qualitative picture of charge doping on these bilayer systems. Doping also creates an electric field in between layers, and in addition, it helps reset the location of the Fermi level. Our results point to additional features to be found experimentally in twisted graphene bilayers.

V. ACKNOWLEDGMENTS

We are grateful to Edward Conrad and Markus E. Kindermann for insightful discussions. We acknowledge the support by the Georgia Tech MRSEC (funded by the National Science Foundation under Grants No. DMR-08-20382) and by the US Department of Energy, Office of Basic Energy Sciences, Division of Materials Sciences and Engineering under Award No. DEFG02-97ER45632. This research used computational resources at the National Energy Research Scientific Computing Center (supported by the Office of Science of the U.S. Department of Energy under Contract No. DE-AC02-05CH11231), and the National Science Foundation TeraGrid (TG-PHY090002).

[1] P. R. Wallace, Phys. Rev. **71**, 622 (1947).
[2] A. H. C. Neto, F. Guinea, N. M. R. Peres, K. S. Novoselov, and A. K. Geim, Rev. Mod. Phys. **81**, 109 (2009).
[3] W. A. de Heer, C. Berger, X. Wu, P. N. First, E. H. Conrad, X. Li, T. Li, M. Sprinkle, J. Hass, M. L. Sadowski, et al., Solid State Commun. **143**, 92 (2007).
[4] J. Hass, F. Varchon, J. E. Millan-Otoya, M. Sprinkle, N. Sharma, W. A. de Heer, C. Berger, P. N. First, L. Magaud, and E. H. Conrad, Phys. Rev. Lett. **100**, 125504 (2008).
[5] P. W. Sutter, J.-I. Flege, and E. A. Sutter, Nature Physics **7**, 406 (2008).
[6] A. Reina, X. Jia, J. Ho, D. Nezich, H. Son, V. Bulovic, M. S. Dresselhaus, and J. Kong, Nano Lett. **9**, 30 (2009).
[7] J. M. B. L. dos Santos, N. M. R. Peres, and A. H. C. Neto, Phys. Rev. Lett. **99**, 256802 (2007).
[8] J. Hass, W. A. de Heer, and E. H. Conrad, J. Phys.: Condens. Matter **20**, 323202 (2008).
[9] M. Sprinkle, D. Siegel, Y. Hu, J. Hicks, A. Tejeda, A. Taleb-lbrahimi, P. L. Fèvre, F. Bertran, S. Vizzini, S. Chiang, et al., Phys. Rev. Lett. **103**, 226803 (2009).

[10] J. Kedzierski, P.-L. Hsu, P. Healey, P. Wyatt, C. Keast, M. Sprinkle, C. Berger, and W. A. de Heer, IEEE Transactions on Electron Devices **55**, 2078 (2008).
[11] J. S. Moon, D. Curtis, M. Hu, D. Wong, C. McGuire, P. M. Campbell, G. Jernigan, J. L. Tedesco, B. VanMil, R. Myers-Ward, et al., IEEE Transactions on Electron Devices **30**, 650 (2009).
[12] Y.-M. Lin, C. Dimitrakopoulos, K. A. Jenkins, D. B. Farmer, H.-Y. Chiu, A. Grill, and P. Avouris, Science **327**, 662 (2010).
[13] A. Tzalenchuk, S. Lara-Avila, A. Kalaboukhov, S. Paolillo, M. Syvajarvi, R. Yakimova, O. Kazakova1, T. J. B. M. Janssen, V. Fal'ko, and S. Kubatkin, Nature Nanotechnology **5**, 186 (2010).
[14] K. S. Kim, Y. Zhao, H. Jang, S. Y. Lee, J. M. Kim, K. S. Kim, J.-H. Ahn, P. Kim, J.-Y. Choi, and B. H. Hong, Nature **457**, 706 (2009).
[15] X. Li, Y. Zhu, W. Cai, M. Borysiak, B. Han, D. Chen, R. D. Piner, L. Colombo, , and R. S. Ruoff, Nano Lett. **9**, 4359 (2009).
[16] S. Latil, V. Meunier, and L. Henrard, Phys. Rev. B **76**, 201402 (2007).
[17] S. Shallcross, S. Sharma, and O. A. Pankratov, Phys. Rev. Lett. **101**, 056803 (2008).
[18] S. Shallcross, S. Sharma, E. Kandelaki, and O. A. Pankratov, Phys. Rev. B **81**, 165105 (2010).
[19] G. T. de Laissardiere, D. Mayou, and L. Magaud, Nano Lett. **10**, 804 (2010).
[20] E. J. Mele, Phys. Rev. B **81**, 161405 (2010).
[21] S. Shallcross, S. Sharma, and O. A. Pankratov, J. Phys.:Condens. Matter **20**, 454224 (2008).
[22] E. McCann, D. S. L. Abergel, and V. I. Fal'ko, Solid State Comm. **143**, 110 (2007).
[23] J. B. Oostinga, H. B. Heersche, X. Liu, A. F. Morpurgo, and L. M. K. Vandersypen, Nature Materials **7**, 151 (2007).
[24] E. S. Morell, J. D. Correa, P. Vargas, M. Pacheco, and Z. Barticevic, Phys. Rev. B **82**, 121407 (2010).
[25] R. Bistritzer and A. H. MacDonald, arXiv:1009.4203 (2010).
[26] R. Bistritzer and A. H. MacDonald, Phys. Rev. B **81**, 245412 (2010).
[27] Z. Ni, Y. Wang, T. Yu, Y. You, and Z. Shen, Phys. Rev. B **77**, 235403 (2008).
[28] P. Poncharal, A. Ayari, T. Michel, and J.-L. Sauvajol, Phys. Rev. B **78**, 113407 (2008).
[29] P. Poncharal, A. Ayari, T. Michel, and J. L. Sauvajol, Phys. Rev. B **79**, 237402 (2009).
[30] D. L. Miller, K. D. Kubista, G. M. Rutter, M. Ruan, W. A. de Heer, P. N. First, and J. A. Stroscio, Science **324**, 924 (2009).
[31] A. Luican, G. Li, J. K. A. Reina, R. R. Nair, K. S. Novoselov, A. K. Geim, and E. Y. Andrei, Phys. Rev. Lett. **106**, 126802 (2011).
[32] J. Hicks, M. Sprinkle, K. Shepperd, F. Wang, A. Tejeda, A. Taleb-Ibrahimi, F. Bertran, P. L. Fèvre, W. A. de Heer, C. Berger, et al., Phys. Rev. B **83**, 205403 (2011).
[33] D. Sun, C. Divin, C. Berger, P. N. First, W. A. de Heer, and T. B. Norris, Phys. Rev. Lett. **104**, 136802 (2010).
[34] J. H. Chen, C. Jang, S. Adam, M. S. Fuhrer, E. D. Williams, and M. Ishigami, Nature Physics **4**, 377 (2008).
[35] A. Bostwick, T. Ohta, T. Seyller, K. Horn, and E. Rotenberg, Nature Physics **3**, 36 (2007).
[36] S. Y. Zhou, D. A. Siegel, A. V. Fedorov, and A. Lanzara, Phys. Rev. Lett. **101**, 086402 (2008).
[37] C. Coletti, C. Riedl, D. S. Lee, B. Krauss, L. Patthey, K. von Klitzing, J. H. Smet, and U. Starke, Phys. Rev. B **81**, 235401 (2010).
[38] T. Ohta, A. Bostwick, T. Seyller, K. Horn, and E. Rotenberg, Science **313**, 951 (2006).
[39] Y. Shi, K. K. Kim, A. Reina, M. Hofmann, L.-J. Li, and J. Kong, ACS Nano **4**, 2689 (2010).
[40] A. Kasry, M. A. Kuroda, G. J. Martyna, G. S. Tulevski, and A. A. Bol, ACS Nano **4**, 3839 (2010).
[41] D. M. Ceperley and B. J. Alder, Phys. Rev. Lett. **45**, 566 (1980).
[42] J. P. Perdew and A. Zunger, Phys. Rev. B **23**, 5048 (1981).
[43] J. M. Soler, E. Artacho, J. D. Gale, A. Garcia, J. Junquera, P. Ordejón, and D. Sanchez-Portal, J. Phys.: Condens. Matter **14**, 2745 (2002).
[44] E. Artacho, E. Anglada, O. Diéguez, J. D. Gale, A. García, J. Junquera, R. M. Martin, P. Ordejón, J. M. Pruneda, D. Sánchez-Portal, et al., J. Phys.: Condens. Matter **20**, 064208 (2008).
[45] N. Troullier and J. L. Martins, Phys. Rev. B **43**, 1993 (1991).
[46] J. Junquera, Phys. Rev. B **64**, 235111 (2001).
[47] R. E. V. Profumo, M. Polini, R. Asgari, R. Fazio, and A. H. MacDonald, Phys. Rev. B **82**, 085443 (2010).